

Article

Improving the Stability of Ru-Doped Ni-Based Catalysts for Steam Methane Reforming during Daily Startup and Shutdown Operation

Tae-Young Kim ^{1,†}, Jong-Heon Lee ^{2,†}, Seongbin Jo ³, Jueon Kim ², Jin-Hyeok Woo ², Ragupathy Dhanusuraman ⁴, Jae-Chang Kim ^{2,*} and Soo-Chool Lee ^{1,*}

¹ Research Institute of Advanced Energy Technology, Kyungpook National University, Daegu 41566, Republic of Korea; tyoung0218@knu.ac.kr

² Department of Chemical Engineering, Kyungpook National University, Daegu 41566, Republic of Korea; rnswwa123@knu.ac.kr (J.-H.L.); lawliet@knu.ac.kr (J.K.); wjh8865@knu.ac.kr (J.-H.W.)

³ Department of Chemical and Environmental Engineering, University of California–Riverside, Riverside, CA 92521, USA; sjo016@ucr.edu

⁴ Nano Electrochemistry Lab (NEL), Department of Chemistry, National Institute of Technology Puducherry, Karaikal 609-609, India; ragu.nitpy@gmail.com

* Correspondence: kjchang@knu.ac.kr (J.-C.K.); soochool@knu.ac.kr (S.-C.L.)

† These authors contributed equally to this work.

Abstract: In this study, a Ru-doped Ni pellet-type catalyst was prepared to produce hydrogen via steam methane reforming (SMR). A small amount of Ru addition on the Ni catalyst improved Ni dispersion, thus affording a higher catalytic activity than that of the Ni catalyst. During the daily startup and shutdown (DSS) operations, the CH₄ conversion of Ni catalysts significantly decreased because of Ni metal oxidation to NiAl₂O₄, which is not reduced completely at 700 °C. Conversely, the oxidized Ni species in the Ru–Ni catalyst can be reduced under SMR conditions because of H₂ spillover from the surface of Ru onto the surface of Ni. Consequently, the addition of a small quantity of Ru to the Ni catalyst can improve the catalytic activity and stability during the DSS operation.

Keywords: Ni pellet-type catalyst; Ru promotion; steam–methane reforming; daily startup and shutdown operation; fuel cell



Citation: Kim, T.-Y.; Lee, J.-H.; Jo, S.; Kim, J.; Woo, J.-H.; Dhanusuraman, R.; Kim, J.-C.; Lee, S.-C. Improving the Stability of Ru-Doped Ni-Based Catalysts for Steam Methane Reforming during Daily Startup and Shutdown Operation. *Catalysts* **2023**, *13*, 949. <https://doi.org/10.3390/catal13060949>

Academic Editors: Kee Young Koo and Unho Jung

Received: 28 April 2023

Revised: 26 May 2023

Accepted: 27 May 2023

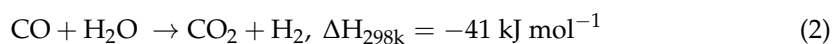
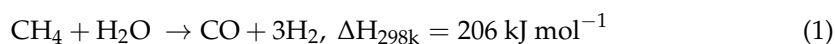
Published: 30 May 2023



Copyright: © 2023 by the authors. Licensee MDPI, Basel, Switzerland. This article is an open access article distributed under the terms and conditions of the Creative Commons Attribution (CC BY) license (<https://creativecommons.org/licenses/by/4.0/>).

1. Introduction

Hydrogen is generally accepted as an attractive alternative to support energy consumption while reducing the environmental impact. Among the energy-generating devices using hydrogen, proton-exchange membrane fuel cells (PEMFC) are appealing devices for residential power generation applications due to their high efficiency and low emission tendency. The reforming of methane is the most common method to produce hydrogen. There are several types of methane reforming, such as steam reforming (SR), dry reforming (DR) and partial oxidation (POx). Among the methane reforming technologies, steam methane reforming (SMR) (Equation (1)) is the most widely used process to produce hydrogen [1–6]. SMR has a high hydrogen yield efficiency (–74%), yielding 4 mol H₂ and 1 mol CO₂ for each methane group (Equations (1) and (2)).



The various noble metal and transition metal-based catalysts for the SMR reaction have been reported [7–22]. Although noble metals (e.g., Ru, Rh and Pt) show excellent catalytic activity and high coke resistance [7,8], they are too expensive to be applied in

industrial SMR. In contrast, Ni-based catalysts show high performance at a lower price. Therefore, Ni catalysts are the most commonly used catalysts on an industrial scale for the SMR processes [5,6,9]. However, Ni-based catalysts are usually deactivated by coking [10], metal sintering [10–12] and oxidation [13,14]. Among them, the oxidation of Ni metal has a negative effect on the reforming catalyst in PEMFC because the catalyst bed in the reformer on a fuel cell is purged with steam for safety reasons between the shutdown and startup. Therefore, the catalyst must be resistant to oxidation, as Ni metal can be oxidized by steam [15,16]. Fortunately, the high activity and stability of the Ni-based catalyst can be improved by adding promoters or alloying with other metals in SMR.

Various oxide supports such as Al_2O_3 , SiO_2 , TiO_2 and CeO_2 have been studied to improve catalytic performance and stability [17]. Al_2O_3 has the advantage of thermal stability and efficient structural characteristics, including strong metal–support interaction [18]. The interaction between active metal and support affects the structure, the crystalline phase, and the dispersion of active sites, facilitating the catalytic performance and stability of catalysts. Kumar et al. prepared the supported Ni catalyst with diverse support for the reforming of the methane reaction [19]. The Al_2O_3 -supported Ni catalyst exhibited well-dispersed small Ni particles, strong Ni–Al interaction, and the best catalytic activities.

Various studies have reported that the addition of noble metals in small quantities improves the stability of Ni-based catalysts [20–23]. Matus et al. reported that the catalytic activity of Ni catalysts was promoted by Pt, Pd, Re and Sn for the autothermal reforming of methane (ATR) [24]. The addition of Pt, Pd and Re led to the self-activation of catalysts under the reaction conditions and an increase in the H_2 yield due to the enhanced reducibility of Ni^{2+} . Jeong et al. reported that a small amount of Ru finely doped over Ni/ Al_2O_3 or Ni/ MgAl_2O_4 facilitated the reduction of NiO species, decreasing the coking of the catalyst in SMR [20]. The Ru-doped Ni catalysts were activated without the prereduction treatment due to their improved reducibility, whereas the unprompted Ni catalysts were activated only after the prereduction treatment with H_2 . Moreover, Takehira et al. reported that 0.05 wt% of the Ru loading on the Ni catalyst effectively suppressed the deactivation in SMR [25]. The Ru– $\text{Ni}_{0.5}/\text{Mg}_{2.5}(\text{Al})\text{O}$ catalysts showed high stability under steam purging since the oxidation of Ni metal by steam was effectively suppressed by the hydrogen spillover from Ru. According to the DFT study, NiRu bimetals showed lower activation energies in alternative reactions that led to the evolution of CO gas, facilitated the decomposition of methane, and improved the evolution of H_2 gas [26].

The pressure drop in the catalyst bed must be considered to operate SMR effectively on an industrial scale. Indeed, powder-type catalysts could lead to a high-pressure drop in a fixed-bed reactor. Therefore, to operate in a fixed-bed reactor, catalytically active components should be supported on an inert, porous pellet to avoid pressure drop. For the catalyst supported on an inert porous pellet, the catalytic performance of a pellet-type catalyst is related to the distribution of catalytically active components. To solve this problem, many studies have been conducted on egg-shaped catalysts [27–30]. In the “eggshell type catalyst”, the catalytically active component is mainly located in the outer region of the pellet. Depending on the strength of the metal precursor–support interaction, the contact time, drying conditions, and various additives can be adjusted to prepare these catalysts. In our previous study, a Ru/ Al_2O_3 eggshell catalyst was prepared for the SMR reaction by adding an inorganic acid that weakens the interaction [28]. Although Ru/ Al_2O_3 eggshell catalysts with the catalytic layers were prepared with various thicknesses, they did not show significant differences in the catalytic performance in SMR. Owing to the weak metal precursor–support interaction between Ni nitrate and Al_2O_3 , the thickness of the catalytic layer on the pellet was controlled by tuning the contact time. In another way, Jang et al. reported a preparation method for the Ni/alumina eggshell catalysts using immiscibility between the hydrophobic solvent preoccupied inside the pellet and the aqueous hydrophilic precursor solution [29]. After drying the solvents and receiving proper thermal treatment, nickel particles were selectively located in the outer region of the pellet.

Recently, we reported that the Ru-based eggshell-type catalysts exhibited high activity and stability during the DSS operation [28]. Nevertheless, several problems exist with Ru-based catalysts, such as cost and availability on an industrial scale. In this study, we developed Ru-doped Ni catalysts on pellet-type alumina to investigate activity and stability during the DSS operation. The effects of Ru addition on SMR activity and stability during the DSS operation were investigated. The catalysts were analyzed using scanning electron microscopy (SEM) with energy-dispersive X-ray spectroscopy (EDS), a high-resolution 2D X-ray diffractometer (HR-2D XRD), temperature-programmed reduction with H₂ (H₂-TPR), Brunauer–Emmett–Teller (BET) analysis, X-ray photoelectron spectroscopy (XPS), and thermogravimetric analysis with H₂ (H₂-TGA).

2. Results and Discussion

2.1. Characterization of the Ni-Based Catalysts

Figure 1 shows external surface and cross-sectional images of Ni/Al₂O₃ and Ru–Ni/Al₂O₃ catalysts using a digital microscope. The external surface of the Ni/Al₂O₃ catalyst exhibited a light blue color, whereas a black color was observed in Ru–Ni/Al₂O₃. The cross-sectional images of both catalysts exhibited a light blue color. The black color was only detected on the outermost surface of Ru–Ni/Al₂O₃. It can be confirmed through the distribution of nickel and ruthenium in the cross-section of both catalysts from the edge to the center, measured via SEM–EDS (Figure S1). For the Ni/Al₂O₃ catalyst, a very high concentration of Ni was detected on the external catalyst surface, and the nickel concentration gradually decreased inside the catalyst (Figure S1a). As shown in Figure S1b, a similar trend was also observed for the Ru–Ni/Al₂O₃ catalyst, but the Ni concentration inside the catalyst was slightly higher than that of the Ni catalyst. It seems that the Ni particles on the external surface of pellets penetrate inside the pellet in the second impregnation step. Ru in the Ru–Ni/Al₂O₃ catalyst was supported only on the external pellet surface due to strong Ru precursor–support interaction, as seen in the cross-sectional image.

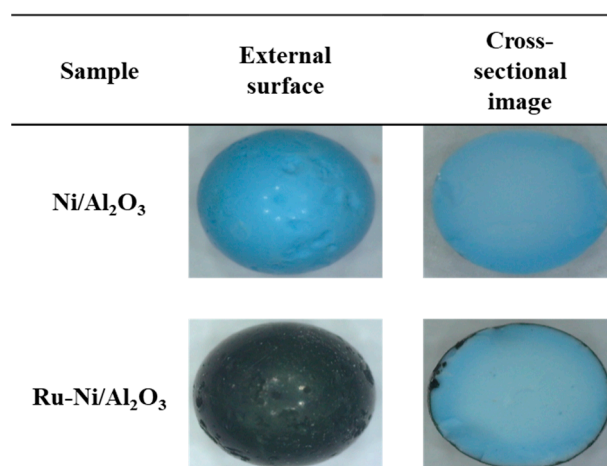


Figure 1. External surface, cross-sectional images of Ni/Al₂O₃ and Ru–Ni/Al₂O₃ catalysts.

High-resolution two-dimensional X-ray diffraction (HR-2D XRD) was used to study the structural properties on the surface of Ni/Al₂O₃ and Ru–Ni/Al₂O₃ catalysts in fresh and reduced states (Figure 2). Figure 2a shows the XRD patterns of Ni/Al₂O₃ catalysts in the fresh and reduced states. For the Ni/Al₂O₃ catalyst, peaks of NiAl₂O₄ (JCPDS No. 10-0339) and γ -Al₂O₃ (JCPDS No. 79-1558) were observed in the fresh state without peaks of NiO due to high calcination conditions. After the H₂ reduction treatment at 800 °C for 3 h, peaks of metallic Ni (JCPDS No. 70-1849) were observed. Additionally, the overlapped peaks of NiAl₂O₄ and γ -Al₂O₃ shifted to peaks of γ -Al₂O₃, indicating that the NiAl₂O₄ phase was reduced to the metallic Ni phase. For the Ni–Ru/Al₂O₃ catalyst (Figure 2b), peaks of RuO₂ (JCPDS No. 88-0286) existed with peaks of NiAl₂O₄ and γ -Al₂O₃. After the

H₂ reduction treatment, the Ni–Ru/Al₂O₃ catalyst also confirmed peaks of metallic Ni and a peak shift of NiAl₂O₄, and metallic Ru (JCPDS No. 65-7645) was additionally observed. In addition, crystallite sizes of Ni metal in reduced catalysts were calculated using the Scherrer equation. The crystallite sizes of Ni metal in Ni/Al₂O₃ and Ru–Ni/Al₂O₃ catalysts were 15.6 nm and 10.9 nm, respectively. Ni–Ru/Al₂O₃ catalyst showed smaller Ni⁰ particle sizes compared to Ni/Al₂O₃ catalyst. It is proposed that adding Ru to the Ni/Al₂O₃ catalyst might enhance the Ni dispersion.

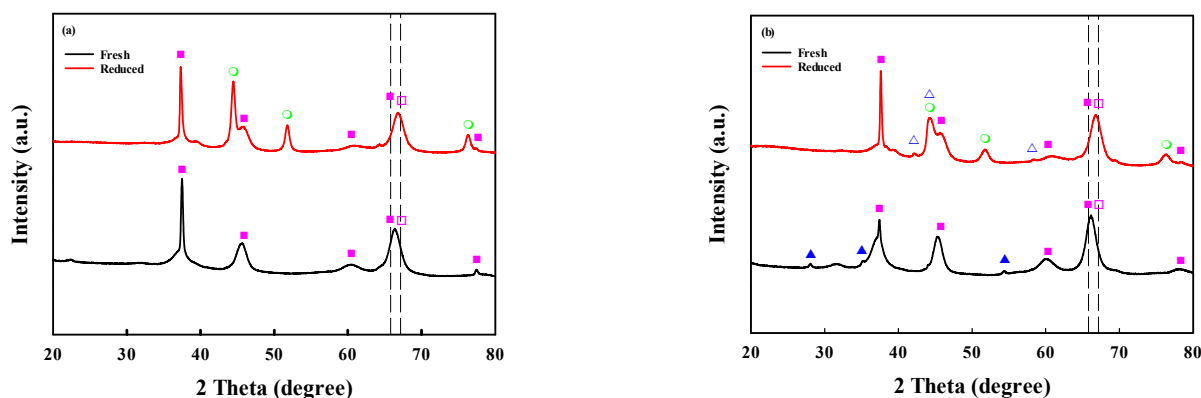


Figure 2. HR-2D XRD patterns of fresh and reduced (a) Ni/Al₂O₃ and (b) Ru–Ni/Al₂O₃ catalysts: (○) metallic Ni, (■) NiAl₂O₄, (□) γ-Al₂O₃, (▲) RuO₂ and (△) metallic Ru.

The H₂-TPR profiles of the Ni-based catalysts were obtained under 10% H₂ at a temperature range of 100 °C to 900 °C with a temperature ramp rate of 10 °C min^{−1} after pretreatment with N₂ at 200 °C for 1 h to desorb the adsorbed gases (Figure 3). The H₂-TPR profiles showed no peaks at temperatures below 500 °C, only peaks at approximately 800 °C due to the reduction of NiAl₂O₄: NiAl₂O₄(s) + H₂(g) ↔ Ni(s) + Al₂O₃(s) + H₂O(g) [18]. Notably, the reduction temperature of NiAl₂O₄ shifted to lower temperatures in the presence of Ru. Jeong et al. reported that the formation of a Ru–Ni alloy resulted in an easy reduction of Ni on the Ru–Ni/Al₂O₃ catalyst [23]. Ni²⁺ particles were reduced by the hydrogen spillover from metallic Ru to form a Ru–Ni alloy on the surface of the metallic Ni particles, indicating that Ru not only increased the dispersion of Ni but also improved its reducibility.

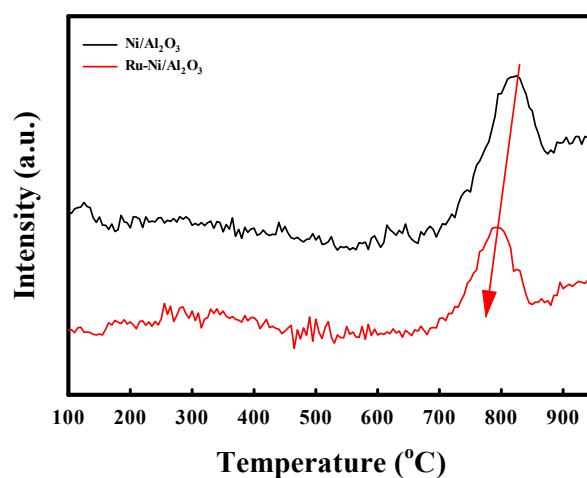


Figure 3. H₂-TPR profiles of the Ni/Al₂O₃ and Ru–Ni/Al₂O₃ catalysts under 10% H₂ conditions from 100 °C to 900 °C at a temperature ramping rate of 10 °C/min.

2.2. Steam Reforming Reaction with Ni-Based Catalysts

SMR reactions were performed on both catalysts at various WHSVs to investigate the effect of Ru addition on the catalytic activity. Figures 4 and S2 show the CH₄ conversion and selectivity of the Ni/Al₂O₃ and Ru–Ni/Al₂O₃ catalysts at various WHSVs. The CH₄ conversions of each catalyst changed dramatically as the WHSV increased from 12,000 mL/g/h to 48,000 mL/g/h. As the WHSV increased, the CH₄ conversion of both catalysts decreased due to the reduction in contact time between the reactant and active site. At low WHSV, the CH₄ conversion of both catalysts was comparable regardless of Ru addition. However, at the highest WHSV (48,000 mL/g/h) under our experimental conditions, the Ru–Ni/Al₂O₃ catalyst showed about 6% higher CH₄ conversion than that of the Ni/Al₂O₃ catalyst. Considering the very low CH₄ conversion over Ru/Al₂O₃ catalyst (0.1 wt% Ru), the increase in Ni dispersion by Ru addition facilitated the formation of CH_x^{−*} and O^{−*}, resulting in an improvement in CH₄ conversion [31]. As shown in Figure S2, at the WHSV (12,000 mL/g/h), the Ni/Al₂O₃ catalyst showed the selectivity of H₂, CO and CO₂ to be 78%, 13% and 9%, respectively. Additionally, the selectivity of Ru–Ni/Al₂O₃ was almost identical to that of the Ni/Al₂O₃ catalyst. It might be that adding Ru to Ni/Al₂O₃ does not affect selectivity during the SMR reaction. As the WHSV increased, the CO₂ selectivity of both catalysts slightly increased because the lower CH₄ conversion increased the H₂O/CO ratio, which caused the WGS reaction [28].

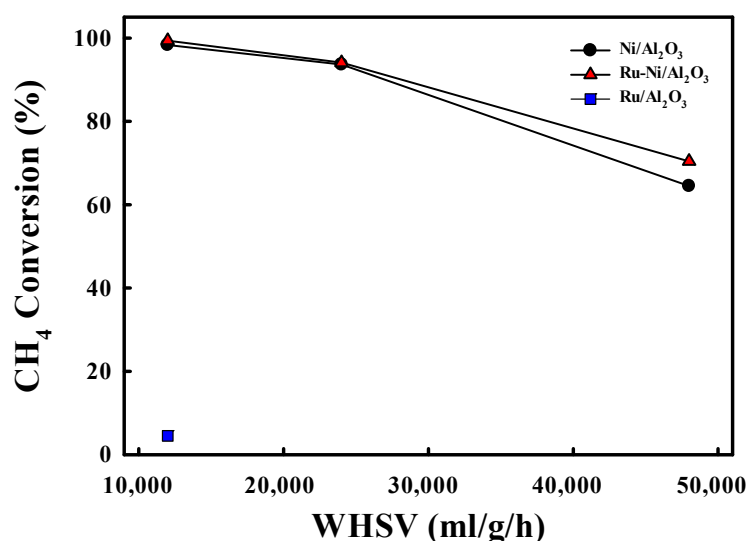


Figure 4. CH₄ conversion with Ni/Al₂O₃, Ru–Ni/Al₂O₃ and Ru/Al₂O₃ catalysts for SMR reactions at various WHSV.

The DSS operations were performed to investigate the long-term stability of Ni/Al₂O₃ and Ru–Ni/Al₂O₃ catalysts for the application of PEMFC. After the pre-reduction, the reaction started in a CH₄/H₂O/N₂ (10/30/60 mL/min) for 90 min at 700 °C, then the temperature was cooled to 200 °C under steam purging with H₂O/N₂ (30/60 mL/min), in which only the CH₄ supply was stopped under reaction conditions. After the reactor temperature was maintained at 200 °C for 30 min, it was then heated to 700 °C under purge conditions. CH₄ gas was added to start the reaction; the reaction was held for 90 min at 700 °C. To investigate the long-term stability of the DSS operation, the SMR reaction and cooling were repeated. Figure 5 shows the CH₄ conversion and selectivity of catalysts during the DSS operation. At the first SMR reaction, the Ni/Al₂O₃ catalyst showed 99% CH₄ conversion, and the selectivity of H₂, CO and CO₂ was 77%, 13% and 9%, respectively. Ru–Ni/Al₂O₃ showed similar values of CH₄ conversion and selectivity compared to Ni/Al₂O₃ catalysts. The Ni/Al₂O₃ catalyst showed a slight decrease in CH₄ conversion after the first DSS operation and significant deactivation after three cycles. In addition, the selectivity of CO and CO₂ changed drastically during DSS operation. The

CO selectivity tended to decrease and the CO₂ selectivity to increase because the low CH₄ conversion induced the WGS reaction as the H₂O/CO ratio increased. Conversely, the CH₄ conversion and selectivity of the Ru–Ni catalyst were maintained during DSS operation. Considering that Ru/Al₂O₃ showed very poor activity and deactivation (Figure S3), a small loading of Ru in Ru–Ni/Al₂O₃ as a promoter could prevent deactivation during the steam purge. As shown in Table 1, in a previous report, the 2 wt%Ru/Al₂O₃ showed a high CH₄ conversion of 99.0% with stability during DSS operation [28]. Compared to 2%Ru/Al₂O₃, the Ru–Ni/Al₂O₃ catalyst (0.1 wt% Ru/10 wt%) also exhibited high CH₄ conversion and stability for SMR during DSS operation. High amounts of H₂ production with cyclic stability can be achieved over Ru–Ni/Al₂O₃ catalysts in DSS operation during SMR by reducing the amount of Ru by 95% (2 to 0.1 wt%). Considering the price of Ru is much higher than Ni, the amount of Ru is the key factor in determining the production costs of catalysts. Therefore, the reduction of the Ru loading amount in the catalyst is expected to improve economic feasibility.

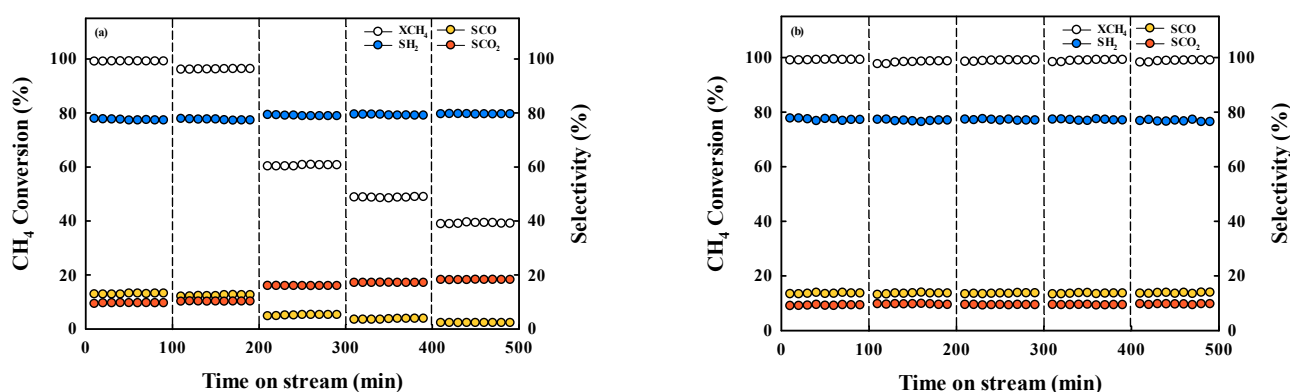


Figure 5. CH₄ conversion and selectivity of (a) Ni/Al₂O₃ and (b) Ru–Ni/Al₂O₃ catalysts during DSS operation.

Table 1. Summary of the catalytic performance of catalysts during DSS operation.

Catalyst	Reaction Condition	Cycle	CH ₄ Conversion (%)	Ref
Ni/Al ₂ O ₃	SV: 12,000 mL/g/h 700 °C	1	99.0	This study
		3	60.2	
		5	38.8	
Ru–Ni/Al ₂ O ₃	SV: 12,000 mL/g/h 700 °C	1	99.1	This study
		3	99.0	
		5	99.0	
2%Ru/Al ₂ O ₃	SV: 12,000 mL/g/h 700 °C	1	99.0	[28]
		3	99.0	
		5	99.0	

Both catalysts were characterized using N₂ adsorption–desorption instrumentation, H₂-TGA, 2D-XRD and XPS to investigate the reasons for the difference in catalyst deactivation during DSS operation. The N₂ adsorption–desorption isotherms and the pore size distributions of catalysts are shown in Figures S4 and S5, respectively. Both catalysts exhibited a type IV isotherm with a hysteresis loop, which is associated with mesoporous structures. After the DSS operation, the pore size distribution of catalysts gradually shifted toward larger pores. This change may suggest that catalysts suffered agglomeration and migration during DSS operation. Moreover, the textural properties of the catalysts are listed in Table 2. The BET surface area, pore volume and pore size of both catalysts indicated similar decreasing trends during DSS operation. It is known that the reduction of textural properties such as BET surface area and volume leads to a decrease in catalytic activity.

Despite the decrease in textural properties of both catalysts, the Ru–Ni/Al₂O₃ catalyst showed stable activity during DSS operation. Therefore, given this trend, it is considered that other factors probably have a greater impact on catalyst deactivation.

Table 2. Texture properties and H₂ consumption of the catalysts before and after DSS operation.

Catalyst	State	BET Surface Area (m ² /g)	Pore Volume (cm ³ /g)	Average Pore Size (nm)	H ₂ Consumption (mmol/g)
Ni/Al ₂ O ₃	Fresh	127.2	0.39	8.1	1.515
	After the 1st DSS	124.3	0.43	9.3	0.189
	After the 5th DSS	105.2	0.38	9.4	0.250
Ru–Ni/Al ₂ O ₃	Fresh	137.0	0.43	8.7	1.578
	After the 1st DSS	130.9	0.43	9.4	0.252
	After the 5th DSS	106.5	0.38	11.6	0.884

High-resolution two-dimensional X-ray diffraction (HR-2D XRD) was analyzed after the DSS operation cycle (Figure 6a,b). For the Ni/Al₂O₃ catalyst, peaks of metallic Ni, NiO, NiAl₂O₄ and γ -Al₂O₃ were observed after the 1st DDS, indicating oxidation of metallic Ni under the steam purge step. The peaks of metallic Ni remained after the 2nd SMR reaction. However, peaks of metallic Ni were not observed after the 5th DSS and 6th reactions. It suggested that the DSS operation step could gradually oxidize the metallic Ni to NiO on the Ni/Al₂O₃ catalyst, and NiO was not reduced under SRM conditions. Therefore, a decrease in CH₄ conversion on the Ni catalyst seems to be due to Ni oxidation during DSS operation and the poor reducibility of Ni species under SRM conditions. On the other hand, for the Ni–Ru/Al₂O₃ catalyst, peaks of metallic Ni, metallic Ru, NiAl₂O₄ and γ -Al₂O₃ were observed without peaks of NiO after the 1st DDS. The sharp peak of metallic Ni was still observed after the 2nd reaction. After the 5th DSS, the peaks of NiO on the Ru–Ni/Al₂O₃ catalyst were detected, indicating metallic Ni was oxidized because of repeated exposure to steam during DSS operation. However, it was observed that NiO can be reduced to metallic Ni during the 6th SMR reaction.

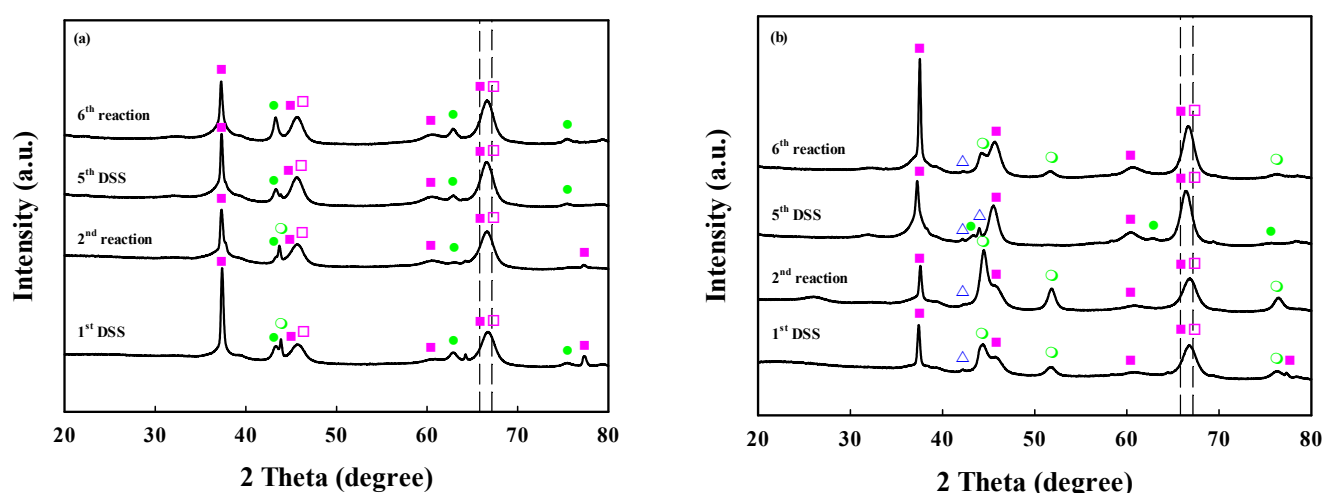


Figure 6. HR-2D XRD patterns of (a) Ni/Al₂O₃ and (b) Ru–Ni/Al₂O₃ catalysts during DSS operation: (●) Ni oxide, (○) metallic Ni, (■) NiAl₂O₄, (□) γ -Al₂O₃ and (△) metallic Ru.

XPS analyses of Ni/Al₂O₃ and Ru–Ni/Al₂O₃ catalysts were conducted to determine the valence states of the Ni species after DSS operation. Figure 7 shows the Ni 2p_{3/2} spectra of Ni/Al₂O₃ and Ru–Ni/Al₂O₃ catalysts after reduction and DSS operation. For the reduced catalysts, the three peaks of the Ni 2p_{3/2} spectra ranging from 873 to 847 eV were observed. The first peak at 852.7 eV corresponds to the Ni⁰, the peak at 855.5 eV corresponds

to the Ni^{2+} , and the last peak at 861.5 eV corresponds to the satellite peak [32]. For the Ru–Ni/ Al_2O_3 catalysts, the peak intensity of Ni^0 was much higher compared to Ni/ Al_2O_3 , due to the better reducibility. After the 5th DSS, the peak of Ni^0 was not observed on the Ni/ Al_2O_3 catalyst, whereas the Ni^0 peak was still observed on the Ru–Ni/ Al_2O_3 catalyst, suggesting that the addition of Ru to the Ni/ Al_2O_3 catalyst could suppress the oxidation of the Ni species after continuous DSS operation.

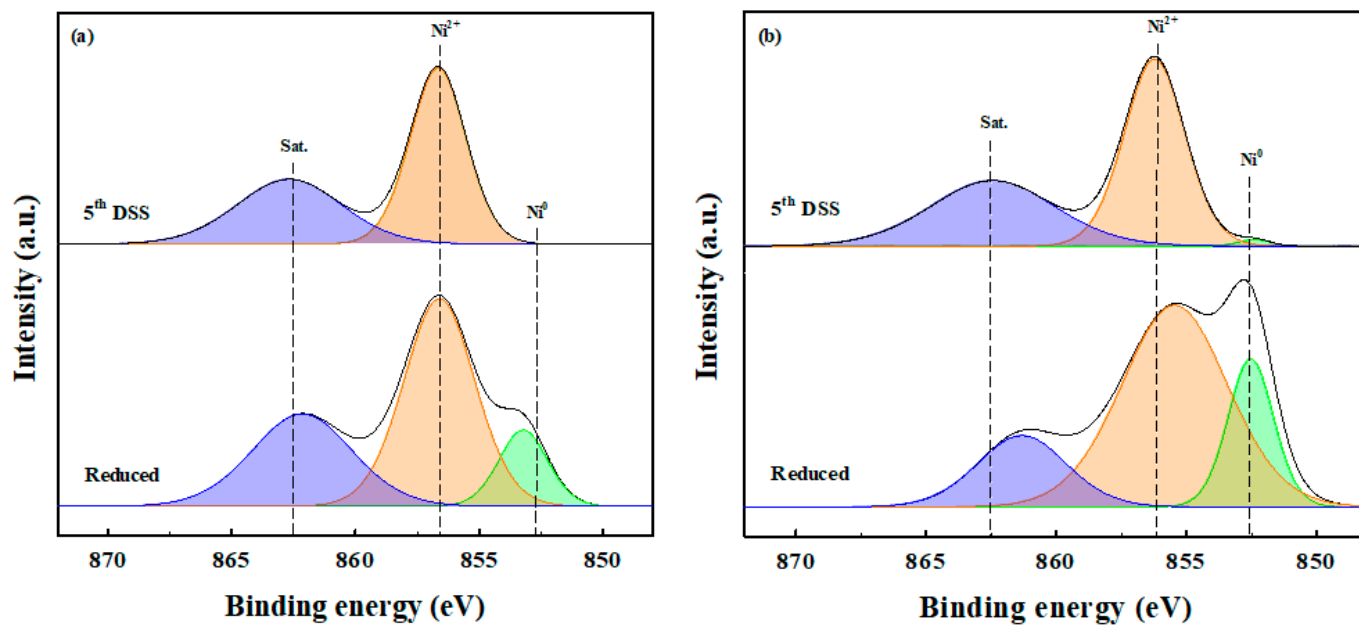


Figure 7. XPS spectra of Ni $2p_{3/2}$ of the (a) Ni/ Al_2O_3 and (b) Ru–Ni/ Al_2O_3 catalysts during the DSS operation cycle.

In addition, H_2 -TGA was conducted to investigate the differences in the reducibility of both catalysts. Firstly, the fresh and spent catalysts were heated to 800 °C and 700 °C, respectively, under N_2 gas. Then, while maintaining the temperature, the N_2 gas was changed to H_2 gas to reduce the catalysts for 2 h. As shown in Table 2, fresh Ni/ Al_2O_3 and Ru–Ni/ Al_2O_3 catalysts showed H_2 consumption amounts of 1.515 and 1.578 mmol/g, respectively, which are similar to the theoretical maximum value in the 10 wt% Ni catalyst (1.704 mmol/g). After the 1st DDS, Ni/ Al_2O_3 and Ru–Ni/ Al_2O_3 catalysts exhibited low H_2 consumption amounts of 0.189 and 0.252 mmol/g, respectively, compared to fresh samples. It might be because the metallic Ni on catalysts was not oxidized significantly in the first steam purging step. For the Ni/ Al_2O_3 catalyst, H_2 consumption after the 5th DSS was identical to that after the 1st DSS, regardless of the Ni oxidation state. On the other hand, the Ru–Ni/ Al_2O_3 catalyst exhibited a relatively high amount of H_2 consumption (0.884 mmol/g) to reduce NiO formed during continuous DSS operation, compared to the Ni/ Al_2O_3 catalyst. As mentioned in H_2 -TPR, Ru further assisted the Ni reduction in the Ru–Ni/ Al_2O_3 catalyst due to easy H_2 dissociation on Ru, followed by a spillover of hydrogen to Ni. Thus, it is worth noting that adding Ru to the Ni/ Al_2O_3 catalyst can suppress the oxidation of Ni during steam purge conditions and enhance reducibility, resulting in cyclic stability during DSS operation.

3. Materials and Methods

3.1. Materials

The Ni(II) nitrate hexahydrate ($\text{Ni}(\text{NO}_3)_2 \cdot 6\text{H}_2\text{O}$) and Ru(III) nitrosyl nitrate ($\text{Ru}(\text{NO}_3)_3(\text{NO})$, Ru 31.3% min) were purchased from AlfaAesar (Ward Hill, MA, USA). Spherical-shaped γ - Al_2O_3 pellets were purchased from SASOL (Sandton, South Africa).

3.2. Catalyst Synthesis

All catalysts were synthesized via impregnation methods. Before preparation, the pellet was dried at 150 °C for 2 h. The concentration of Ni metal was 10 wt% based on Ni/Al₂O₃. The desired amounts of pellets and Ni(NO₃)₂·6H₂O were dispersed in deionized (DI) water, and the mixture was continuously stirred for 1 h. The mixed solution was evaporated in a drying oven at 150 °C for 5 h and calcined in a muffle furnace under air at 700 °C for 4 h with a temperature ramping rate of 10 °C/min. Ru-added Ni catalyst was prepared by a two-step impregnation method. The desired amounts of calcined Ni/Al₂O₃ and Ru(NO₃)₃(NO) were dispersed in DI water and stirred for 1 h. The concentration of Ru metal was 0.1 wt% based on Ru–Ni/Al₂O₃. The Ru–Ni/Al₂O₃ catalyst was dried at 150 °C for 5 h and calcined at 700 °C for 4 h. 10 wt% Ni catalyst, 0.1 wt% Ru–10 wt% Ni catalyst, and 0.1 wt% Ru catalyst are designated as Ni/Al₂O₃, Ru–Ni/Al₂O₃ and Ru/Al₂O₃, respectively. The steps of the catalyst preparation are presented in Figure S6.

3.3. Characterization

The cross-sectional images of catalysts after preparation were observed using a Dino-Lite Premier Digital Microscope (AM3113T, ANMO Electronics Corp., New Taipei City, Taiwan). The temperature-programmed reduction (TPR) profiles of the Ni-based catalysts were obtained under 10% H₂ treatments from 100 °C to 900 °C at a temperature ramping rate of 10 °C/min. The outlet gases were recorded via gas chromatography (GC) equipped with thermal conductivity detectors (TCD). The change in the catalytically active components inside the alumina pellet was measured via field-emission scanning electron microscopy (FE-SEM, SU-8230, Hitachi, Tokyo, Japan) with EDS (Oxford Instruments). HR-2D XRD measurements were performed using a Bruker D8 Discover High-Resolution X-ray diffractometer (Korea Basic Science Institute, Daegu, Republic of Korea) with a VANTEC500 (2D detector) and Cu K α radiation filtered by a Montel mirror operated at 40 kV and 40 mA. The surface area, pore volume and pore size were measured by the BET method using ASAP2020 (Micromeritics Instrument Co., Norcross, GA, USA). H₂-TGA was conducted at 700 °C or 800 °C to determine the H₂ consumption of the fresh and spent catalysts, respectively, and the results were recorded using the SDT Q600. X-ray photoelectron spectroscopy (XPS) was used to obtain surface chemical states on the surface of catalysts in an X-ray photoelectron spectrometer using a NEXSA (ThermoFisher, Waltham, MA, USA) equipped with an Al K α source.

3.4. Steam–Methane Reforming Tests

The steam–methane reforming tests were determined by monitoring their concentrations via GC. The Ni-based pellet-type catalysts (0.5 g) were packed into a fixed-bed reactor with a diameter of $\frac{1}{2}$ an inch and placed in an electric furnace at atmospheric pressure. A thermocouple was placed at the center of the catalyst bed. Prior to the steam–methane reforming, 10 vol% H₂ and balanced N₂ at 100 mL/min (WHSV: 12,000 mL/g/h) were passed through the packed bed at 800 °C for 3 h to reduce the catalysts. After H₂ pretreatment, the gas composition was changed to pure N₂ to purge H₂ from the reactor for 2 min. During the SMR test, the reaction temperatures were maintained at 700 °C, and the gas composition was changed to 30 vol% H₂O, 10 vol% CH₄ (steam/carbon ratio: 3), and balance N₂ at 100 mL/min. In the DSS operation (Figure 8), the catalysts were cooled to 200 °C at a rate of 10 °C/min under purge conditions after a 90-min reaction. The purge condition consisted of H₂O/N₂ (30/60 mL/min), wherein only the CH₄ supply was stopped under reaction conditions. The catalyst bed temperature was maintained at 200 °C for 30 min and later increased to 700 °C under purge conditions. CH₄ gas was added to start the reaction, and the reaction was performed again for 90 min. To perform the DSS operation, this reaction was repeated five times.

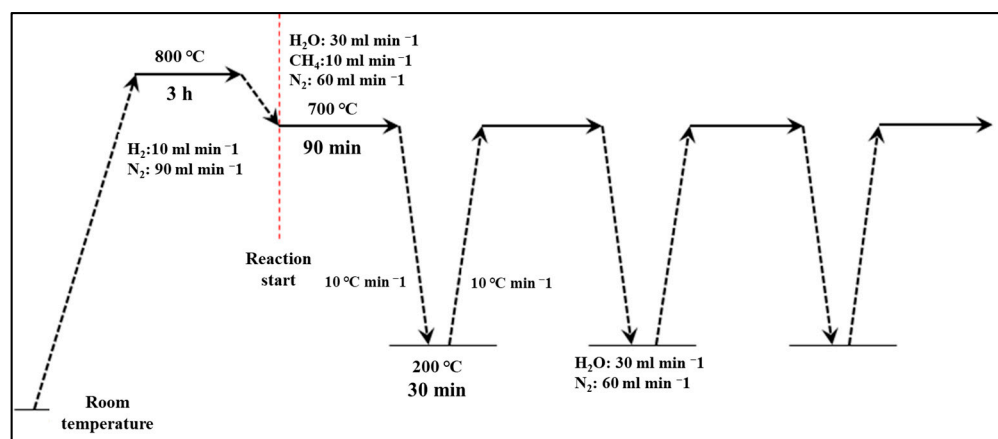


Figure 8. Diagram of the DSS operation in the SMR reaction.

The inlet and outlet lines of the reactor were maintained at 120 °C using a heating tape to prevent the condensation of water vapor. Furthermore, the reactor outlet stream was passed through a condenser to capture water before entering the reactor and GC column. The dried gases were analyzed using a gas chromatograph (Agilent 6890) equipped with two TCDs. The first Carboxen 1000 packed column was connected to a TCD for analysis of N₂, CO, CH₄ and CO₂ gases, and the second one was connected to the other TCD for H₂ gas analysis.

The conversion of CH₄ (X_{CH_4}) and selectivity of the products (CO, CO₂ and H₂) were calculated using Equations (3)–(6) as follows:

$$X_{CH_4} = \frac{F_{CH_4}^{in} - F_{CH_4}^{out}}{F_{CH_4}^{in}} \times 100 \quad (3)$$

$$S_{CO} = \frac{F_{CO}^{out}}{F_{CO}^{out} + F_{CO_2}^{out} + F_{H_2}^{out}} \times 100 \quad (4)$$

$$S_{CO_2} = \frac{F_{CO_2}^{out}}{F_{CO}^{out} + F_{CO_2}^{out} + F_{H_2}^{out}} \times 100 \quad (5)$$

$$S_{H_2} = \frac{F_{H_2}^{out}}{F_{CO}^{out} + F_{CO_2}^{out} + F_{H_2}^{out}} \times 100. \quad (6)$$

4. Conclusions

In this study, Ni/Al₂O₃ and Ru–Ni/Al₂O₃ catalysts were prepared to produce hydrogen via steam–methane reforming and tested in DSS operation. The prepared catalysts were characterized by SEM–EDS, HR-2D XRD, H₂-TPR, N₂-physisorption, XPS and H₂-TGA. Compared to Ni/Al₂O₃ catalyst, Ru–Ni/Al₂O₃ catalyst showed high Ni dispersion and enhanced reducibility due to the interaction between Ni and Ru metal and hydrogen spillover from Ru. Therefore, the Ru–Ni/Al₂O₃ catalyst showed higher catalytic activity than the Ni/Al₂O₃ catalyst at high WHSV (48,000 mL/g/h). As the DSS cycle progressed, the methane conversion of Ni catalysts significantly decreased, whereas Ru–Ni/Al₂O₃ exhibited sustainable activity. In fact, the repeated DSS operation turned out to partially oxidize the Ni metal and reduce the texture properties of Ni/Al₂O₃ and Ru–Ni/Al₂O₃ catalysts. Although Ni metal on the Ru–Ni/Al₂O₃ catalyst was oxidized, oxidized nickel can be reduced better because Ru can spillover hydrogen into nearby Ni sites. Consequently, adding Ru to the Ni catalyst could be beneficial for the stability of the catalyst by enhancing the reducibility, resulting in the re-reduction of NiO on the catalyst surface.

Supplementary Materials: The following supporting information can be downloaded at: <https://www.mdpi.com/article/10.3390/catal13060949/s1>, Figure S1. Metal concentration profile measured in prepared catalysts by SEM-EDS: (a) Ni/Al₂O₃ and (b) Ru-Ni/Al₂O₃ catalysts; Figure S2. Selectivity of catalysts for SMR reactions at various WHSV: (a) Ni/Al₂O₃ and (b) Ru-Ni/Al₂O₃ catalysts; Figure S3. CH₄ conversion of Ru/Al₂O₃ catalysts for SMR reaction during DSS operation; Figure S4. The N₂ adsorption–desorption isotherms of catalysts: (a) Ni/Al₂O₃ and (b) Ru-Ni/Al₂O₃ catalysts; Figure S5. The pore size distributions of catalysts: (a) Ni/Al₂O₃ and (b) Ru-Ni/Al₂O₃ catalysts; Figure S6. The scheme of the preparation of catalysts by the impregnation method.

Author Contributions: Conceptualization, T.-Y.K. and J.-H.L.; formal analysis, J.-H.L., S.J., J.-H.W., J.K. and R.D.; investigation, J.-H.L., T.-Y.K., J.K. and R.D.; supervision, S.-C.L. and J.-C.K.; writing—original draft, T.-Y.K. and J.-H.L.; writing—review and editing, T.-Y.K. and S.-C.L. All authors have read and agreed to the published version of the manuscript.

Funding: This work was supported by the Korea Institute of Energy Technology Evaluation and Planning (KETEP) and the Ministry of Trade, Industry & Energy (MOTIE) of the Republic of Korea (20213030030240).

Data Availability Statement: The data presented in this study are available on request from the corresponding author. Data are contained within the article or Supplementary Materials.

Conflicts of Interest: The authors declare no conflict of interest.

References

1. Carapellucci, R.; Giordano, L. Steam, dry and autothermal methane reforming for hydrogen production: A thermodynamic equilibrium analysis. *J. Power Sources* **2020**, *469*, 228391. [CrossRef]
2. Bian, Z.; Wang, Z.; Jiang, B.; Hongmanorom, P.; Zhong, W.; Kawi, S. A review on perovskite catalysts for reforming of methane to hydrogen production. *Renew. Sustain. Energy Rev.* **2020**, *134*, 110291. [CrossRef]
3. Summa, P.; Samoeden, B.; Motak, M. Dry and steam reforming of methane. Comparison and analysis of recently investigated catalytic materials. A short review. *Pol. J. Chem. Technol.* **2019**, *21*, 31–37. [CrossRef]
4. Torimoto, M.; Ogo, S.; Hisai, Y.; Nakano, N.; Takahashi, A.; Ma, Q.; Seo, J.G.; Tsuneki, H.; Norby, T.; Sekine, Y. Support effects on catalysis of low temperature methane steam reforming. *RSC Adv.* **2020**, *10*, 26418–26424. [CrossRef]
5. Cho, E.; Yu, Y.J.; Kim, Y.; Phan, T.N.; Park, D.; Ko, C.H. Egg-shell-type Ni supported on MgAl₂O₄ pellets as catalyst for steam methane reforming: Enhanced coke-resistance and pellet stability. *Catal. Today* **2020**, *352*, 157–165. [CrossRef]
6. Cho, E.H.; Koo, K.Y.; Lee, H.W.; Park, Y.-K.; Yoon, W.L.; Ko, C.H. Preparation of egg-shell-type Ni/Ru bimetal alumina pellet catalysts: Steam methane reforming for hydrogen production. *Int. J. Hydrog. Energy* **2017**, *42*, 18350–18357. [CrossRef]
7. Khani, Y.; Shariatnia, Z.; Bahadoran, F. High catalytic activity and stability of ZnLaAlO₄ supported Ni, Pt and Ru nanocatalysts applied in the dry, steam and combined dry-steam reforming of methane. *Chem. Eng. J.* **2016**, *299*, 353–366. [CrossRef]
8. Jones, G.; Jakobsen, J.G.; Shim, S.S.; Kleis, J.; Andersson, M.P.; Rossmesl, J.; Abild-Pedersen, F.; Bligaard, T.; Helveg, S.; Hinnemann, B. First principles calculations and experimental insight into methane steam reforming over transition metal catalysts. *J. Catal.* **2008**, *259*, 147–160. [CrossRef]
9. Lee, H.; Lee, D. Synthesis Chemistry and Properties of Ni Catalysts Fabricated on SiC@Al₂O₃ Core-Shell Microstructure for Methane Steam Reforming. *Catalysts* **2020**, *10*, 391. [CrossRef]
10. Iglesias, I.; Forti, M.; Baronetti, G.; Mariño, F. Zr-enhanced stability of ceria based supports for methane steam reforming at severe reaction conditions. *Int. J. Hydrog. Energy* **2019**, *44*, 8121–8132. [CrossRef]
11. Morales-Cano, F.; Lundegaard, L.F.; Tiruvalam, R.R.; Falsig, H.; Skjøth-Rasmussen, M.S. Improving the sintering resistance of Ni/Al₂O₃ steam-reforming catalysts by promotion with noble metals. *Appl. Catal. A Gen.* **2015**, *498*, 117–125. [CrossRef]
12. Dehghan-Niri, R.; Walmsley, J.C.; Holmen, A.; Midgley, P.A.; Rytter, E.; Dam, A.H.; Hungria, A.B.; Hernandez-Garrido, J.C.; Chen, D. Nanoconfinement of Ni clusters towards a high sintering resistance of steam methane reforming catalysts. *Catal. Sci. Technol.* **2012**, *2*, 2476–2484. [CrossRef]
13. Guo, Y.; Zhou, L.; Kameyama, H. Steam reforming reactions over a metal-monolithic anodic alumina-supported Ni catalyst with trace amounts of noble metal. *Int. J. Hydrog. Energy* **2011**, *36*, 5321–5333. [CrossRef]
14. Li, D.; Nakagawa, Y.; Tomishige, K. Methane reforming to synthesis gas over Ni catalysts modified with noble metals. *Appl. Catal. A Gen.* **2011**, *408*, 1–24. [CrossRef]
15. Payne, B.; Biesinger, M.; McIntyre, N. The study of polycrystalline nickel metal oxidation by water vapour. *J. Electron Spectrosc. Relat. Phenom.* **2009**, *175*, 55–65. [CrossRef]
16. Natesakhawat, S.; Watson, R.B.; Wang, X.; Ozkan, U.S. Deactivation characteristics of lanthanide-promoted sol-gel Ni/Al₂O₃ catalysts in propane steam reforming. *J. Catal.* **2005**, *234*, 496–508. [CrossRef]
17. Zolghadri, S.; Honarvar, B.; Rahimpour, M.R. Synthesis, application, and characteristics of mesoporous alumina as a support of promoted Ni-Co bimetallic catalysts in steam reforming of methane. *Fuel* **2023**, *335*, 127005. [CrossRef]

18. He, L.; Ren, Y.; Yue, B.; Tsang, S.C.E.; He, H. Tuning metal–support interactions on Ni/Al₂O₃ catalysts to improve catalytic activity and stability for dry reforming of methane. *Processes* **2021**, *9*, 706. [[CrossRef](#)]
19. Kumar, R.; Kumar, K.; Choudary, N.; Pant, K. Effect of support materials on the performance of Ni-based catalysts in tri-reforming of methane. *Fuel Process. Technol* **2019**, *186*, 40–52. [[CrossRef](#)]
20. Zhou, L.; Guo, Y.; Zhang, Q.; Yagi, M.; Li, H.; Chen, J.; Sakurai, M.; Kameyama, H. Self-activation and self-regenerative activity of trace Ru-doped plate-type anodic alumina supported nickel catalysts in steam reforming of methane. *Catal. Commun.* **2008**, *10*, 325–329. [[CrossRef](#)]
21. Li, D.; Nishida, K.; Zhan, Y.; Shishido, T.; Oumi, Y.; Sano, T.; Takehira, K. Sustainable Ru-doped Ni catalyst derived from hydrotalcite in propane reforming. *Appl. Clay Sci.* **2009**, *43*, 49–56. [[CrossRef](#)]
22. Guo, Y.; Li, H.; Jia, L.; Kameyama, H. Trace Ru-doped anodic alumina-supported Ni catalysts for steam reforming of kerosene: Activity performance and electrical-heating possibility. *Fuel Process. Technol.* **2011**, *92*, 2341–2347. [[CrossRef](#)]
23. Jeong, J.H.; Lee, J.W.; Seo, D.J.; Seo, Y.; Yoon, W.L.; Lee, D.K.; Kim, D.H. Ru-doped Ni catalysts effective for the steam reforming of methane without the pre-reduction treatment with H₂. *Appl. Catal. A Gen.* **2006**, *302*, 151–156. [[CrossRef](#)]
24. Matus, E.; Sukhova, O.; Ismagilov, I.; Kerzhentsev, M.; Stonkus, O.; Ismagilov, Z. Hydrogen Production through Autothermal Reforming of Ethanol: Enhancement of Ni Catalyst Performance via Promotion. *Energies* **2021**, *14*, 5176. [[CrossRef](#)]
25. Takehira, K.; Ohi, T.; Miyata, T.; Shiraga, M.; Sano, T. Steam reforming of CH₄ over Ni-Ru catalysts supported on Mg-Al mixed oxide. *Top. Catal.* **2007**, *42*, 471–474. [[CrossRef](#)]
26. Yoon, Y.; Kim, H.; Lee, J. Enhanced catalytic behavior of Ni alloys in steam methane reforming. *J. Power Sources* **2017**, *359*, 450–457. [[CrossRef](#)]
27. Pinna, F. Supported metal catalysts preparation. *Catal. Today* **1998**, *41*, 129–137. [[CrossRef](#)]
28. Lee, J.-H.; Jo, S.; Kim, T.-Y.; Woo, J.-H.; Lee, Y.; Kim, M.-S.; Park, H.-O.; Lee, S.-C.; Kim, J.-C. Preparation of Eggshell-Type Ru/Al₂O₃ Catalysts for Hydrogen Production Using Steam-Methane Reforming on PEMFC. *Catalysts* **2021**, *11*, 951. [[CrossRef](#)]
29. Jang, M.-S.; Cho, E.H.; Koo, K.Y.; Yoon, W.L.; Ko, C.H. Facile preparation of egg-shell-type pellet catalysts using immiscibility between hydrophobic solvent and hydrophilic solution: Enhancement of catalytic activity due to position control of metallic nickel inside alumina pellet. *Appl. Catal. A Gen.* **2017**, *530*, 211–216. [[CrossRef](#)]
30. Zhuang, Y.; Claeys, M.; Van Steen, E. Novel synthesis route for egg-shell, egg-white and egg-yolk type of cobalt on silica catalysts. *Appl. Catal. A Gen.* **2006**, *301*, 138–142. [[CrossRef](#)]
31. Laosiripojana, N.; Assabumrungrat, S. Methane steam reforming over Ni/Ce–ZrO₂ catalyst: Influences of Ce–ZrO₂ support on reactivity, resistance toward carbon formation, and intrinsic reaction kinetics. *Appl. Catal. A Gen.* **2005**, *290*, 200–211. [[CrossRef](#)]
32. Lv, Z.; Ruan, J.; Tu, W.; Hu, X.; He, D.; Huang, X.; Qin, C. Integrated CO₂ capture and In-Situ methanation by efficient dual functional Li₄SiO₄@Ni/CeO₂. *Sep. Purif. Technol.* **2023**, *309*, 123044. [[CrossRef](#)]

Disclaimer/Publisher’s Note: The statements, opinions and data contained in all publications are solely those of the individual author(s) and contributor(s) and not of MDPI and/or the editor(s). MDPI and/or the editor(s) disclaim responsibility for any injury to people or property resulting from any ideas, methods, instructions or products referred to in the content.